Nanoscale

Accepted Manuscript

This article can be cited before page numbers have been issued, to do this please use: A. Yadav, R. Pandey, T. Liao, V. S. Zharinov, K. Hu, J. Vernieres, R. E. Palmer, P. Lievens, D. Grandjean and Y. Shacham-Diamand, *Nanoscale*, 2020, DOI: 10.1039/C9NR09730A.

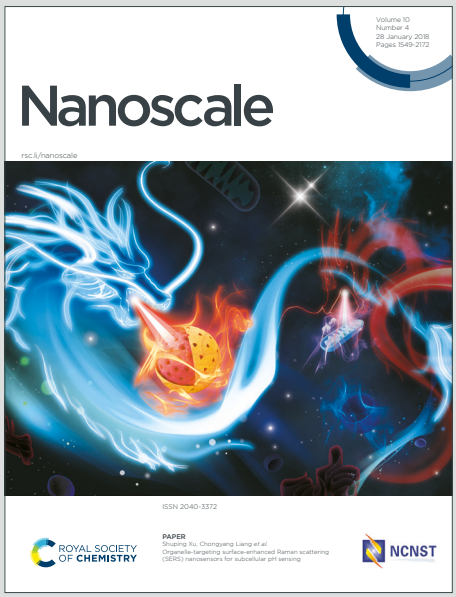

ROYAL SOCIETY OF CHEMISTRY

rsc.li/nanoscale

View Article Online
DOI: 10.1039/C9NR09730A

ARTICLE

Platinum-nickel bimetallic nanoclusters ensemble-on-polyaniline nanofilm for enhanced electrocatalytic oxidation of dopamine

Received 00th January 20xx,
Accepted 00th January 20xx

DOI: 10.1039/x0xx00000x

Anupam Yadav[a*†], Richa Pandey[b*†], Ting-Wei Liao[a], Vyacheslav S. Zharinov[a], Kuo-Juei Hu[a], Jerome Vernieres[c], Richard E. Palmer[c], Peter Lievens[a], Didier Grandjean[a*], Yosi Shacham-Diamand[d]

We report a new approach to design flexible functional material platforms based on electropolymerized polyaniline (PANI) polymer nanofilms modified with bimetallic nanoclusters (NCs) for efficient electro-oxidation of small organic molecules. Composition defined ligand free $Pt_{0.75}Ni_{0.25}$ NCs were synthesized in gas phase using the Cluster Beam Deposition (CBD) technology and characterized using RTOF, HAADF-STEM, XAFS and XPS. NCs were then directly deposited on PANI coated templates to construct eletrodes. Dopamine (DP) molecule was used as representative organic analyte and the influence of NCs-PANI hybrid's atomistic structure on the electrochemical and electrocatalytic performance was investigated. As prepared, nearly monodispersed, $Pt_{0.75}Ni_{0.25}$ NCs of ca. 2 nm diameter featuring a PtOx surface combined with a shallow platelet like Ni-O(OH) phase formed a densely packed active surface on PANI at ultralow metal coverages. Electrochemical measurements (EIS and CV) show a 2.5 times decrease in charge transfer resistance and a remarkable 6-fold increase at lower potential in the mass activity for $Pt_{0.75}Ni_{0.25}$ NCs in comparison to their pure Pt counterparts. The enhanced electrochemical performance of the $Pt_{0.75}Ni_{0.25}$ NCs hybrid interface is ascribed to the formation of mixed Pt metal and Ni-O(OH) phases at the surface of the alloyed PtNi cores of the bimetallic NCs under electrochemical conditions combined with an efficient charge conduction pathway between NCs.

Introduction

Current state of the art electrodes for (bio)electrochemical systems such as biosensors, microbial fuel cell and related electrochemical applications are generally made from (100 - 200 nm) thin films of Pt or Au owing to their high catalytic activity, biocompatibility and functionalization propensity.[1, 2] However, the primary challenge of such Pt and Au based devices is to produce highly active, stable and conducting latforms at low cost for their widespread application. Most of the recent efforts have been dedicated towards minimizing the usage and enhancing the performance of scarce and expensive Pt and Au metals through nanostructuring. The two main strategies are (1) dispersing them as nanoparticles (NPs) on inexpensive supports and (2) combining them with a second metal such as earth abundant Ni with Pt to synergistically enhance their activity while lowering their cost.[3]

Conducting Polymers (CP) are inexpensive flexible materials that have been used for developing diverse applications.[4, 5] Among the large family of CPs, Polyaniline (PANI) has been investigated extensively.[6, 7] The low cost of the aniline precursor,[8] its facile synthesis in aqueous environments,[9] flexible[10] and tuneable electrical and electrochemical properties[11] make PANI a perfect material to design, develop and optimize new material solutions for bioelectronics and energy devices fabrication.[12-14] Moreover, PANI is electrochemically reversible and more resistant to electrode fouling than inflexible carbon paste and bare glassy carbon solid state electrodes.[15] Modification of PANI with metal NPs such as Pt,[16-18] Au,[19-21] Ag,[22-24] Pd,[25, 26] and Ni[27-29] further expands its properties and usage.[30] More generally NP modified PANI (PANI-NP)[31,35,52-55] inherits enhancement in conductivity and electrocatalytic activity and in return imparts NPs good electrochemical stability. However, a controlled, non-destructive and stable integration of NPs (especially that of well-defined bimetallic NPs) with PANI remains a major challenge.[12, 31, 32] Most of the (electro)chemical methods used for PANI-NP fabrication are complex and do not allow a homogenous and precise combination of two components either due to the aggregation of NPs or the limited solubility of

[a] Quantum Solid State Physics, Department of Physics and Astronomy, KU Leuven, Celestijnenlaan 200D, B-3001 Leuven, Belgium
[b] Department of Engineering Physics, Faculty of Engineering, McMaster University, Hamilton- L8S 4L8, Canada
[c] College of Engineering, Swansea University, Bay Campus, Fabian Way, Swansea SA1 8EN, United Kingdom.
[d] Department of Physical Electronics, School of Electrical Engineering, and Department of Materials Science and Engineering, Faculty of Engineering, Tel Aviv University, Ramat Aviv, Tel Aviv- 69978, Israel

† Anupam Yadav and Richa Pandey contributed equally to the manuscript.
* Emails to: Anupam.yadav@kuleuven.be, pander2@mcmaster.ca and Didier.grandjean@kuleuven.be

Electronic Supplementary Information (ESI) available: This file includes supporting surface as well as electrochemical characterization study relevant to understand the information provided in the manuscript [Ni-K edge EXAFS structural refinements, XPS spectra of O1s and Binding Energies tables, Randles EIS spectra model]. See DOI: 10.1039/x0xx00000x

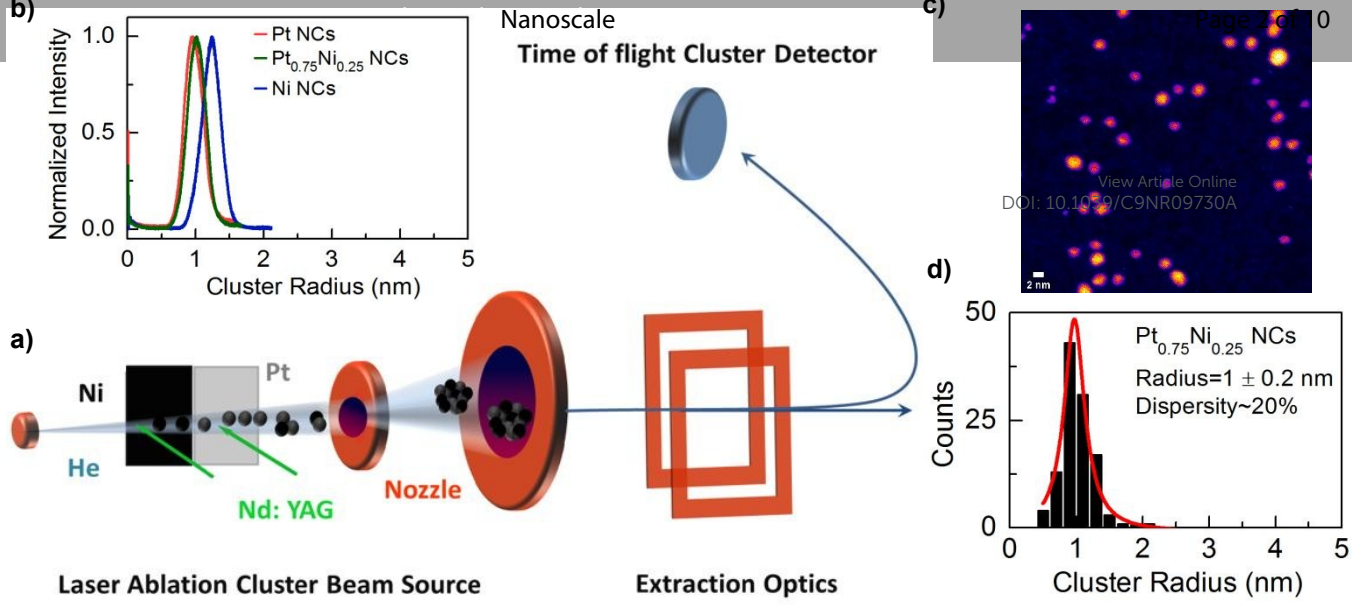

Figure 1: (a) Illustration of the Laser Ablation based Cluster Beam Deposition Set up (b) Time of Flight mass spectrometry size distribution of bimetallic $Pt_{0.75}Ni_{0.25}$, pure Pt and Ni NCs; (c) STEM-HAADF image of $Pt_{0.75}Ni_{0.25}$ NCs on carbon TEM grids; (d) Histogram of the radius distribution of $Pt_{0.75}Ni_{0.25}$ NCs deposited on carbon TEM grids.

PANI in any solvent.[33-39] This inhomogeneity further hinders the thorough characterization and understanding of the physicochemical properties of such hybrid materials. This understanding is crucial to develop enhanced electro-oxidation of small organic molecules for advanced (bio)electrochemical applications.

DP is a unique electroactive organic molecule from the family of biogenic amines. It is present in central nervous, renal, hormonal and cardiovascular systems and plays a vital role in drug addiction, Alzheimer's and Parkinson's diseases. Additionally, DP has recently gained interest for ex-vivo and in-vivo technical applications. DP is also shown to mediate electron transfer for efficient bioenergy harvesting.[40] DP's oxidative product dopaminoquinone is a starting material for the synthesis of polydopamine that is finding broad applications due to its super hydrophilic, adhesive and semiconducting properties.[41,42-44] Therefore, controlled design of low cost hybrid material platforms for electrochemical applications such as Dopamine (DP) electro-oxidation is required.

In the present work we have produced novel hybrid materials based on PtNi bimetallic nanoclusters (NCs) deposited on PANI by CBD and characterized for their electrochemical and electrocatalytic properties. The structure and morphology are investigated using a combination of reflectron time-of-flight (RToF) mass spectrometry, scanning transmission electron microscopy operated in high angle annular dark field mode (STEM-HAADF), X-ray absorption fine structure spectroscopy (XAFS), X-ray photoelectron spectroscopy (XPS) and scanning electron microscopy (SEM). The PANI-NCs hybrid electrochemical performance towards standard Ferri-Ferro redox couple and Dopamine as representative molecule is characterized by electrochemical impedance measurements (EIS) and cyclic voltammetry (CV), respectively, at neutral pH. We show that by simultaneously controlling the intrinsic electro-catalytic activity of NCs through alloying and the functionality of the modified electrode through the NCs coverage on PANI surface we produce high performance flexible PANI-PtNi NCs hybrid architectures for (bio)electrochemical applications.

Results and discussion

Bimetallic $Pt_{0.75}Ni_{0.25}$ NCs were directly deposited under Ultra High Vacuum (UHV) conditions using CBD on Transmission Electron Microscopy (TEM) grids, SiO_2/Si wafers and electro-polymerized PANI nanofilms (~500 nm) supported on flat Au/Ti/Si substrates. As illustrated in Figure 1a CBD is a solvent- and therefore effluent-free method to produce well defined NCs with pristine surfaces in comparison to NPs synthesized by solvent or electrochemistry-based methods. In-situ RToF mass spectrometry was used to monitor the NCs size distribution and optimize the CBD source conditions to obtain a 2 nm NCs diameter. Figure 1b shows the adjusted size distribution of $Pt_{0.75}Ni_{0.25}$ NCs along with monometallic Pt and Ni reference NCs before deposition. The NCs radii were extracted by converting specific mass distribution of charged NCs into the NCs size distribution under the assumption that all cationic

NCs have +1 charge and are spherical in shape with NC radius ($r_{cluster}$) using the equation below

$$r_{cluster} = \left(\frac{3\,(m/z)}{16\pi\, m_{at}}\right)^{\frac{1}{3}} a$$

$Pt_{0.75}Ni_{0.25}$ and monometallic Ni NCs show damped oscillations with respect to Ni foil and NiO confirming their nanosize (Figure 2a). The similar profiles of both XANES spectra indicate that the local structure of Ni atom sites does not alter substantially upon mixing with Pt in the used atomic ratio of 1:3. A red shift of 0.2 eV in the edge position of $Pt_{0.75}Ni_{0.25}$ NCs

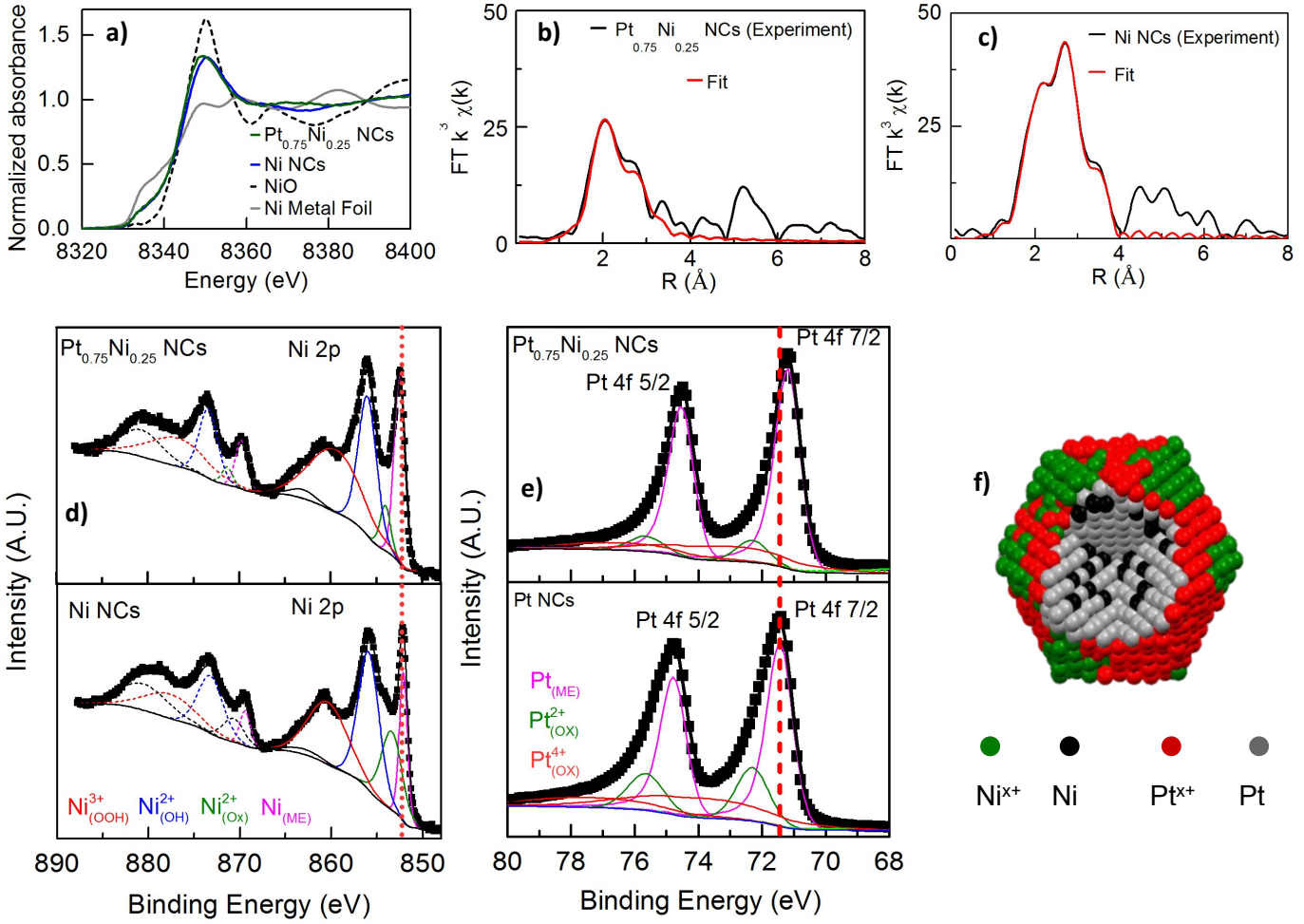

Figure 2: a) Ni K edge XANES of $Pt_{0.75}Ni_{0.25}$ along with Ni NCs, Ni foil and NiO references; Best fit of Fourier Transforms of fluorescence-detected Ni K-edge k^3-weighted EXAFS of b) $Pt_{0.75}Ni_{0.25}$ NCs and c) pure Ni NCs deposited on a SiO_2/Si wafer; d) and e) XPS spectra of Ni 2p 3/2 and Pt 4f core levels of $Pt_{0.75}Ni_{0.25}$ NCs (top panel in d and e), Ni NCs (bottom panel in d) and Pt NCs (bottom panel in e); f) Scheme 1-Model structure of $Pt_{0.75}Ni_{0.25}$ NCs. Green (Ni^{x+}), Black (Ni), Red (Pt^{x+}), Grey (Pt)

where a is the unit cell length (0.392 nm for Pt and 0.352 nm for Ni), m_{at} is atomic mass and m/z is mass to charge ratio. $Pt_{0.75}Ni_{0.25}$ NCs deposited on a carbon TEM grid (Figure 1c) measured with HAADF-STEM (High-Angle Annular Dark-Field Scanning Transmission Electron Microscopy) are nearly monodispersed. This is confirmed by their sharp size distribution histogram determined from the analysis of the images of more than 100 objects that is presented in Figure 1d. The mean NCs size is estimated to be ca. 2 nm in diameter corresponding closely to the NCs mean radii derived from RToF spectra confirming that NCs largely retain their original size upon deposition.

Structural and electronic properties of $Pt_{0.75}Ni_{0.25}$ NCs deposited on silicon wafer were characterized with XAFS. Ni K-edge XANES (X-ray Absorption Near Edge Structure) of with respect to their Ni monometallic counterparts is observed suggesting the presence of a smaller fraction of nickel oxides in the bimetallic $Pt_{0.75}Ni_{0.25}$ NCs. The white line intensity of Ni K edge XANES is also slightly higher in $Pt_{0.75}Ni_{0.25}$ NCs suggesting that different types of nickel oxides are present in both samples. Detailed fitting of the EXAFS gave deeper insights in the NCs structure. The summary of structural parameters obtained from fitting EXAFS spectra of bimetallic $Pt_{0.75}Ni_{0.25}$ and pure Ni NCs is given in Table S1. Fourier transforms (FTs) of the corresponding EXAFS, with best fit presented in Figures 2b and 2c, consists of a main multi-peak in both samples. The shoulder at ca. 2 Å corresponds to a Ni-O contribution (N1) consisting of 2.0 and 2.4 O at 1.99-2.01 Å in bimetallic $Pt_{0.75}Ni_{0.25}$ and pure Ni NCs, respectively, indicating that fractions of ca. 33% to 40% (2/6 and 2.4/6) of Ni atoms are oxidized in an octahedral oxygen coordination. The lower

View Article Online DOI: 10.1039/C9NR09739A

fraction of nickel oxides observed in bimetallic $Pt_{0.75}Ni_{0.25}$ NCs is in line with the red shift observed in the Ni K edge XANES of $Pt_{0.75}Ni_{0.25}$ NCs and further suggests that Ni is largely surrounded by Pt atoms. The Ni-O bond distance of 2.015 Å in pure Ni and 1.99 Å in $Pt_{0.75}Ni_{0.25}$ NCs, shorter than in NiO (Ni-O 2.08 Å) and β-$Ni(OH)_2$ (Ni-O 2.06 Å), suggest the presence of a mixture of Ni oxide with a majority of β-NiOOH (Ni-O 1.9 and 2.07 Å) hydroxide phase in both NCs. A larger fraction of β-NiOOH is found in $Pt_{0.75}Ni_{0.25}$ NCs as indicated by the shorter Ni-O distance found in bimetallic NCs.

The second contribution in the multi-peaks for both samples is a shell (N2) of 1.8 Ni atoms at 2.46 Å in pure Ni and 0.8 Ni atoms at 2.48 Å in bimetallic NCs, respectively. An additional third shell of 2 Pt atoms at 2.66 Å (N3) could be included in the $Pt_{0.75}Ni_{0.25}$ system. Ni-Ni distances similar to those found in Ni metal (2.48 Å[45]) indicate the presence of a fraction of ca. 60 % of a pure metallic phase in monometallic Ni NCs and ca. 67% of a mixture of pure Ni metal and Pt-rich Ni-Pt alloy in bimetallic $Pt_{0.75}Ni_{0.25}$ NCs. In $Pt_{0.75}Ni_{0.25}$ NCs, from the total number of atoms composing the NC, ca. 8.5% are oxidized Ni atoms, 6.5% form a pure Ni metal phase, and 10% are Ni atoms alloyed with Pt. In pure Ni NCs the fit was completed by 2 Ni contributions at 2.91 Å (N4) and 3.40 Å (N5) corresponding to an average of the Ni-Ni distance found in NiO (2.95 Å) and in Ni hydroxide (2.86 Å) and to the second neighbour shell Ni-Ni distances in Ni metal (3.45 Å), respectively.[46] The absence of any of these contributions in $Pt_{0.75}Ni_{0.25}$ NCs suggests the presence of platelet-like shallow patches of highly oxidized Ni oxyhydroxides mostly at the NCs (sub)surface. Given that Ni (1.8) is less electronegative than Pt (2.2), Ni atoms are plausibly more oxidized by surrounding Pt atoms in the bimetallic than in pure Ni NCs. This is supported by the occurrence of larger white line intensity in XANES of $Pt_{0.75}Ni_{0.25}$ NCs despite the smaller fraction of oxidized Ni obtained from EXAFS refinement.

Surface electronic properties of $Pt_{0.75}Ni_{0.25}$ NCs deposited on SiO_2/Si were additionally investigated with XPS to characterize Pt and Ni electronic states. High-resolution XPS spectra along with their best fit components in the Ni 2p 3/2 and Pt 4f core levels regions of the $Pt_{0.75}Ni_{0.25}$ NCs in comparison to their pure Ni and Pt analogues are shown in Figure 2d and 2e. Ni 2p 3/2 spectrum was deconvoluted by 4 peaks identifying the presence of metallic, oxide (+2), hydrous oxide (+2) and oxy-hydrous oxide (+3) Ni phases, shown in Figure 2d. On the other hand, Pt 4f spectrum was best fitted by 3 peaks that could be assigned, respectively, to Pt metal, oxide (+2) and dioxide (+4) (Figure 2e). $Pt_{0.75}Ni_{0.25}$ NCs have less oxidized Ni and Pt atoms in total. Furthermore, the surface of $Pt_{0.75}Ni_{0.25}$ NCs consists of a larger fraction of higher oxide/hydroxide species in comparison to pure Ni and Pt NCs. The relative integrated area of the XPS peaks indicates that in $Pt_{0.75}Ni_{0.25}$ NCs 94% of the surface Ni oxides is composed of $Ni(OH)_2$ and NiOOH phases as compared to 75% in pure Ni NCs, whereas 74% of total surface Pt oxides is PtO_2 as compared to 60% in pure Pt NCs. This analysis is in line with the short Ni-O bond distances determined by EXAFS in $Pt_{0.75}Ni_{0.25}$ (1.99 Å) compared to pure Ni (2.01 Å). The oxide phase distribution was confirmed by fitting of high resolution O 1s spectra of pure Ni, Pt and $Pt_{0.75}Ni_{0.25}$ NCs with Si-O, Ni-O and Pt-O interaction peaks (Figure S3).

The Binding Energies (BEs) in $Pt_{0.75}Ni_{0.25}$ and pure Pt and Ni NCs are summarized in Table S2. XPS analysis shows that the BE of metal Ni 2p increases from 852.1 eV in pure Ni to 852.3 eV in $Pt_{0.75}Ni_{0.25}$ NCs, likely ascribed to a loss of electrons by Ni atoms, and indicates that Ni sites in the bimetallic are more oxidized than in the pure Ni NCs in agreement with the EXAFS analysis. Meanwhile, the BE of Pt 4f decreases from 71.4 eV to 71.1 eV demonstrating likely a gain of electrons by Pt in $Pt_{0.75}Ni_{0.25}$ NCs. Though BE changes can be easily ascribed to charge transfer between the two elements they could also be tied to the surface electronic band modification by the neighbouring hetero element, and the different oxide fractions within the NCs.[47]

XPS in combination with XAFS reveals the complex structure of $Pt_{0.75}Ni_{0.25}$ NCs consisting of disordered NiO_xH_y and PtO_x phases on the surface of an underlying Pt-Ni alloyed core with an increasing Pt concentration from the core towards the surface, as is schematically presented in Figure 2f. This physical structure is further supported by the HAADF-STEM image of a $Pt_{0.75}Ni_{0.25}$ NC that is shown in Figure S4.This is also in line with the atomic ordering observed in Au-Ag bimetallic systems[47] prepared using the same method resulting from a four-step growth process in which the alloyed core of NCs is enriched in the minority element. The proposed heterostructure with a Ni enriched PtNi alloyed core of $Pt_{0.75}Ni_{0.25}$ NCs is consistent with that of Au-Ag architecture, confirming the general character of previous findings from our lab that an overall composition of NCs directly controls their atomic arrangement.[47]

The as-fabricated PANI-$Pt_{0.75}Ni_{0.25}$ NCs hybrid material was then used to construct electrodes that were investigated for their electrochemical properties and electrocatalytic performance. Electropolymerized PANI surfaces were precisely modified with 1.5 and 12 atomic monolayers (1 ML = 1 *10^{15} total atoms per cm^2) deposited as NCs of 2 nm Pt, Ni and $Pt_{0.75}Ni_{0.25}$ NCs. SEM images of these PANI coated flat Au substrates before and after their modification by $Pt_{0.75}Ni_{0.25}$ NCs are presented in Figure 3 a-c. As seen in Figure 3b the pristine PANI nanofilm present a contorted surface morphology fully conformed over the underlying Au surface with an uneven flowing shape and smooth edges. $Pt_{0.75}Ni_{0.25}$ NCs deposited with coverage of 1.5 ML on the PANI film remain highly dispersed and appear nearly isolated on the surface (Figure 3a). Upon increasing the coverage to 12 ML, (Figure 3b) $Pt_{0.75}Ni_{0.25}$ NCs form a densely packed assembly on top of the PANI surface.

Potassium ferricyanide (III) and potassium ferrocyanide (II) couple and the DP molecule were used as representative analytes. Pure Pt and pure Ni NCs counterparts produced in gas phase were used as reference. Figure 3d & 3f (top and bottom) show the EIS measurements of PANI with and without 12 ML of Pt, Ni, $Pt_{0.75}Ni_{0.25}$ NCs using 10mM Fe^{+3}/Fe^{+2} cyanide probe in 0.1M PBS solution (pH~7.2), whereas Figure 3e & 3g (top and bottom) show the comparison of hybrid electrode at different $Pt_{0.75}Ni_{0.25}$ NCs coverages. PANI shows a typical behaviour of capacitor and resistor in series. The behaviour of the NCs deposited PANI can be explained by the simple Randles circuit model (Figure S4). Among the three investigated NCs, pure Ni shows the highest charge transfer resistance (175 Ω), followed by Pt (75 Ω) and $Pt_{0.75}Ni_{0.25}$ (30 Ω). Upon increasing the NCs coverage to 12 ML the PANI-$Pt_{0.75}Ni_{0.25}$ NCs hybrid results in a remarkable 100 times decrease in the charge transfer resistance compared to the 1.5 ML coverage (Figure 3e).

Cyclic Voltammograms (CVs), presented in Figure 4, delineate the electrocatalytic performance of these hybrid electrodes. Figure 4a shows the CVs of hybrid electrodes in DP free 0.1M PBS solution. None of the electrodes show a prominent electrocatalytic signal confirming the absence of electroactive species in the electrolyte. Potential CV scans under neutral pH

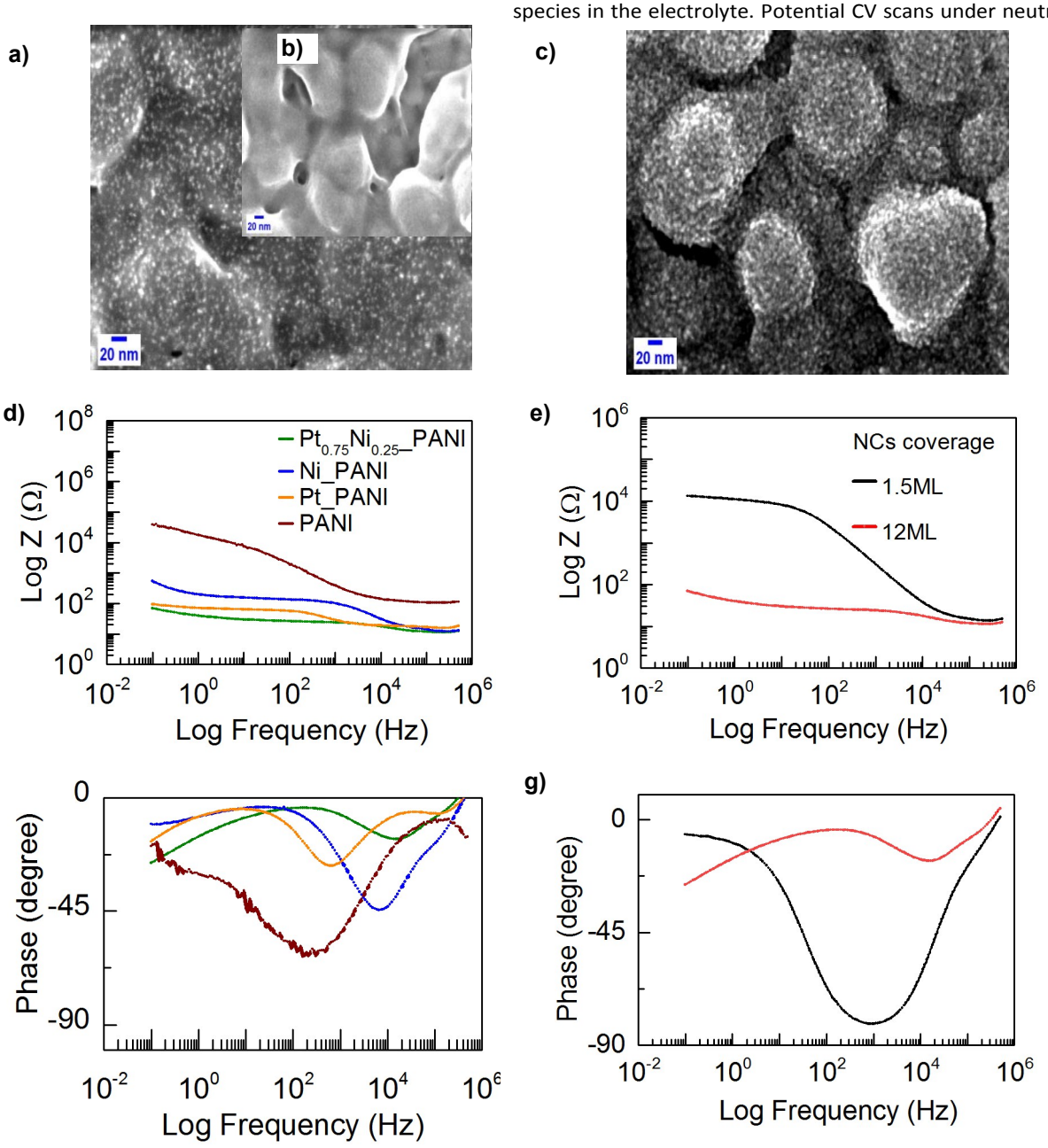

Figure 3:(a-c) SEM images of PANI-NCs hybrid films (a) PANI modified with 1.5 atomic ML $Pt_{0.75}Ni_{0.25}$ NCs coverage with inset image (b) unmodified PANI and (c) PANI modified with 12 atomic ML $Pt_{0.75}Ni_{0.25}$ NCs coverage (d-g) Bode plot of d) and f) of 12ML of $Pt_{0.75}Ni_{0.25}$ (green), Pt (orange), Ni (blue) and PANI (brown). e) and g) $Pt_{0.75}Ni_{0.25}$ of 12 ML (red) and 1.5 ML (black) NCs coverage in 10 mM Fe^{+3}/Fe^{+2} in 0.1 M PBS.

environment of PANI-Pt electrode shows typical features of bulk Pt surface[48] that are absent in those of PANI-$Pt_{0.75}Ni_{0.25}$ and PANI-Ni electrodes. Figure 4b highlights the oxidation and reduction of DP on bare PANI and PANI-Ni, Pt, $Pt_{0.75}Ni_{0.25}$ NCs hybrid electrodes. Upon addition of DP, the absence of redox peaks for bare PANI and PANI-Ni hybrid demonstrates their inability to oxidize or reduce dopamine. The high charge transfer resistance and the absence of electrocatalytic activity of PANI-Ni electrodes towards DP suggests that ultra-low loading of Ni NCs deposited on the external surface of PANI are likely unstable under electrochemical conditions as they may detach from the electrode surface and (or) get strongly passivated with the solution anions.

As observed in the CV of PANI-Pt NCs hybrid, the oxidation of DP occurs at 0.45 V and its reduction at -0.1 V. The Ipa/Ipc ratio around 1.5 depicts an irreversible behaviour. CV of PANI-$Pt_{0.75}Ni_{0.25}$ NCs shows a clear DP oxidation potential shift to a lower value of 0.19 V compared to 0.45 V for its monometallic Pt counterparts. The peak potential difference ΔEp also shifts to 0.1 V from 0.4 V. $Pt_{0.75}Ni_{0.25}$ NCs efficiently catalyse the oxidation of DP, and mediate the transport of electrons through PANI likely by a polaron and bipolaron formation.[49]

The DP oxidation under applied potential may proceed by the loss of H^+ from the DP molecule and the formation of dopaminoquinone on the NCs catalyst surface as illustrated by scheme 1 in Figure 4c.[50] A 3 orders of magnitude high oxidation current is observed for $Pt_{0.75}Ni_{0.25}$ NCs when compared to monometallic Pt NCs leading to a remarkable 6-fold increment in the mass activity at even a lower Pt usage. The calculated mass activities of Pt and $Pt_{0.75}Ni_{0.25}$ NCs and their respective electrochemical surface areas (ECSA) are listed in Table 1. Note that the mass activity for the oxidation peak current is calculated from the specific mass of Pt in pure Pt and $Pt_{0.75}Ni_{0.25}$ NCs. Stability of the electro-catalytic performance of the hybrid electrodes was further confirmed by chronoamperometry (CA) measurements (Figure 4d). A wide dynamic linear DP electro-oxidation current response was observed for both pure Pt and $Pt_{0.75}Ni_{0.25}$ NCs hybrid electrodes under a DP concentration range of 5 to 50 µM implying that these NCs-PANI hybrid electrodes can be applied and further optimized for DP detection. Additionally, the decrease in the Faradaic current from 0.4 mA to 0.1 mA for Pt and $Pt_{0.75}Ni_{0.25}$ NCs respectively observed in the DP-free PBS electrolyte (Figure S5) further supports the occurrence of different surface properties in pure Pt and $Pt_{0.75}Ni_{0.25}$ NCs already evidenced by their distinct CV profiles in the DP-free electrolyte.

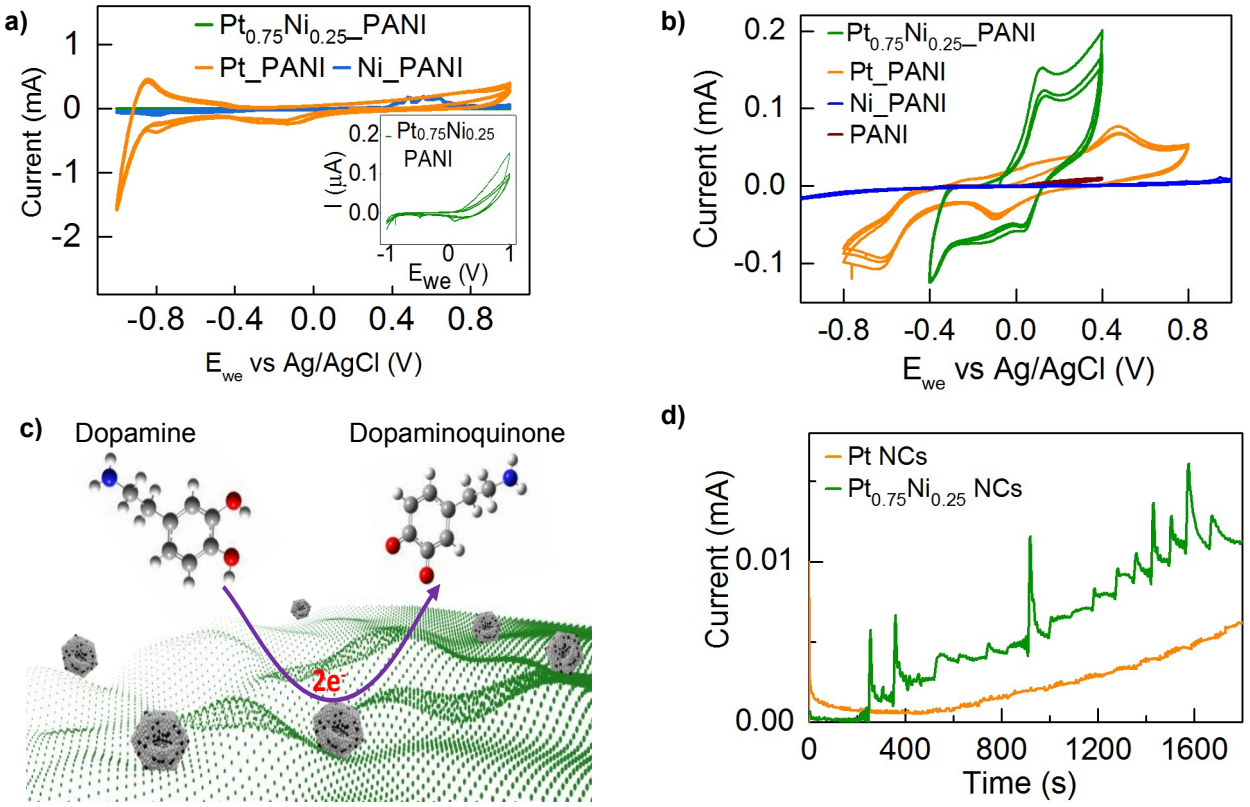

Figure 4: Cyclic voltammogram of PANI (brown), Pt (orange), Ni (blue) and $Pt_{0.75}Ni_{0.25}$ (Green) NCs hybrid electrodes with 12 ML NCs coverages in the absence of DP (a), with the inset showing an enlarged view of $Pt_{0.75}Ni_{0.25}$ NCs, and in the presence (b) of 2mM DP in 0.1 M PBS at 50 mV s^{-1}. (c) The electrochemical oxidation reaction of DP into dopaminoquione (DQ).(d) Chronoamperometric measurement of DP on 12ML Pt (orange) and $Pt_{0.75}Ni_{0.25}$ (green) NCs supported PANI electrodes in PBS solution.

View Article Online
DOI: 10.1039/C9NR09730A

To relate the excellent activity of $Pt_{0.75}Ni_{0.25}$ NCs to the nature and structure of their surface under electrochemical condition we compared the CV profiles of pure Ni, Pt and $Pt_{0.75}Ni_{0.25}$ NC-PANI hybrid electrodes measured in absence of DP. (Figure 4a) The surface structure of NCs under operating conditions differs substantially from that characterized ex situ.[51] In pure Pt NCs a broad feature appearing at -0.1V corresponds to the progressive oxidation of Pt through the adsorption of OH on its extended surface [52, 53] while the single broad peak at - 0.8 V shows the desorption of hydrogen on Pt terrace sites.[52, 54-56] On the contrary, in bimetallic $Pt_{0.75}Ni_{0.25}$ NCs the absence of this H desorption feature suggests the absence of well-defined surface Pt facets and/or that an alternative pathway for hydrogen desorption has been provided for the Pt phase.[48] Pt surfaces are more reduced as suggested by the late onset of surface oxidation visible only above 0.2 V. It is likely that presence of a substantial amount of Ni oxides at the surface of NCs observed ex situ by XAFS and XPS is disrupting the formation of Pt metal extended planes. Besides, the reduced capacitive current in PtNi compared to pure Pt further indicates the increased stability of Pt atoms in bimetallic NCs against electrochemical fouling.

Table 1: Electrocatalytic performance of hybrid materials for oxidation of 2mM DP at 50 mV s^{-1}.

Hybrid Materials	Ipa (A)	ECSA (cm^2)	Specific mass (g/cm^2)	Mass activity ($mA/(g/cm^2)$)
PANI-Pt NCs	6.50E-05	2.21E-04	6.36E-06	2.26
PANI-$Pt_{0.75}Ni_{0.25}$ NCs	1.43E-04	4.86E-04	4.83E-06	14.4

A clear synergetic effect between Pt and Ni at the atomic level that enhances the electro-catalytic performance of bimetallic $Pt_{0.75}Ni_{0.25}$ NCs is demonstrated by EIS and CV measurements. The decrease in the charge transfer resistance, the shift of DP oxidation potentials to 0.19 V from 0.45 V, the higher DP oxidation currents and the enhanced electrochemical stability of $Pt_{0.75}Ni_{0.25}$ NCs compared to their Pt and Ni monometallic counterparts confirm the superior electrochemical properties of bimetallic NCs modified PANI interface. This may be explained by the presence of (sub)surface Ni atoms that enhances the electrocatalytic activity of the Pt surface sites by modifying the local d-band charge carrier density facilitating the activation of the DP molecule on NCs surface. Additionally, the shallow platelet-like Ni-O(OH) present on the $Pt_{0.75}Ni_{0.25}$ NCs surface may further improve the NCs performance through a competing self-redox ($Ni^{2+} \rightarrow Ni^{3+}$) process. This is supported by the increased oxidation currents and the lowered redox potentials observed at the $Pt_{0.75}Ni_{0.25}$ NCs-PANI interface. The effect of $Pt_{0.75}Ni_{0.25}$ NCs coverage was investigated for 1.5 and 12 ML to evaluate their electrochemical response at singly-dispersed versus ensemble level on the PANI surface, respectively (Figure 3a & 3c). PANI-$Pt_{0.75}Ni_{0.25}$ NCs at 12 ML coverage feature structures that are 100 times more efficient in charge transfer compared to the 1.5 ML coverage (Figure 3e). A dense packing of NCs at higher coverage (shown in Figure 3c) likely leads to an improved electron percolation in the NCs assembly and better electron transport through the PANI nanofilm. The diffusion tail corresponding to a Warburg element observed in $Pt_{0.75}Ni_{0.25}$ NCs at 12 ML coverage (Figure 3g) can be attributed to the increased electrode surface roughness. The large enhancement of the electrochemical properties of these flexible hybrid PANI-PtNi NC materials stems from a combination of favourable alloying within the NCs with an optimal density of NCs at the surface of PANI allowing an efficient conduction pathway.

Conclusions

We have reported the controlled and designed synthesis of a novel PANI-PtNi NCs hybrid electrode consisting of well-defined $Pt_{0.75}Ni_{0.25}$ NCs produced by CBD and deposited directly onto electropolymerized PANI nanofilms at ultralow precious metal loadings. Bimetallic $Pt_{0.75}Ni_{0.25}$ NCs demonstrated superior electrochemical and electrocatalytic characteristics that are attributed to the presence of a combination of reduced Pt atoms with a platelet-like Ni-O(OH) phase on the NCs surface furnishing better electronic conductivity. Practical implementation and performance assessment of such flexible NCs-PANI hybrid material with complex analytes are underway. Our results demonstrate that bimetallic NCs-PANI based flexible hybrid architectures are promising materials for future (bio)electrochemical applications.

Experimental Methods

Materials

Ultra-Holey Carbon TEM grids (Ted Pella) and SiO_2/Si wafers for STEM and XAFS-XPS measurements were used, respectively. Nickel foil (99.9%) and Nickel oxide (99.9%, Sigma-Aldrich) were used as references for synchrotron experiments. An aqueous solution of Aniline (99.5%, Fluka) and Potassium nitrate (KNO_3, 99%) was used for the electro-polymerization of PANI. Potassium Ferricyanide ($K_3[Fe(CN)_6]$, Merck) and Potassium Ferrocyanide ($K_4[Fe(CN)_6]$, Merck) redox couples were used in the preliminary electrochemical study of the hybrid PANI-NCs electrode. Sodium chloride (NaCl, Merck), Potassium chloride (KCl, Merck), Potassium dihydrogen phosphate (KH_2PO_4, Merck) and Di-sodium hydrogen phosphate (Na_2HPO_4, Sigma-Aldrich) were used to prepare the Phosphate buffer saline (PBS). Dopamine hydrochloride ($C_8H_{12}ClNO_2$, 98%, Sigma-Aldrich) constituted the analyte of interest. Deionized water (DI water) was used throughout the studies.

DOI: 10.1039/C9NR09730A

Designed synthesis of PANI-PtNi NCs hybrid interface

The hybrid electrode is fabricated by sputtering Au (200 nm) /Ti (15 nm) on silicon 2 × 1 cm substrate. This Au film acts as the seed layer for the electropolymerization of PANI. The bath prepared for the electrochemical polymerization contained an aqueous solution of 0.1 M Aniline and 0.1 M KNO_3 dissolved in aqueous solution with pH adjusted to 6.5. A Pt plate and a KCl saturated calomel electrode were employed as the auxiliary and reference electrode, respectively, for the electro-polymerization of PANI. PANI films (500 nm) were grown by sweeping the potential between -0.2 to 9 V with a sweep rate of 50 mV cm^{-2}.

NCs were directly deposited on PANI nanofilms using CBD. NCs beams were produced in an UHV environment by ablating a Pt-Ni alloy target (75:25 atomic percent, purity 99.95%, ACI alloy) with a pulsed laser (10 Hz, Nd:YAG laser, Spectra-Physics, INDI). The target was placed in a sample holder arranged in a leak-proof assembly within the CBD source. Details of the laser ablation NCs source are given elsewhere. [57, 58] In brief, material plasma is generated when the target surface is irradiated by a laser pulse. This material plume is rapidly quenched by Helium gas pulse within the liquid nitrogen cooled source block, resulting in the condensation of atoms and NCs formation. By varying the condensation conditions such as the pressure of He pulsed gas and the temperature of the CBD source, the NCs size can be fine-tuned. The free regime effluence of the mostly neutral NCs on expansion through the replaceable nozzle head is skimmed and collimated and finally soft-landed on PANI coated electrodes (1cm*1cm) and other supports at 300 K under 10^{-9} mbar pressure in the deposition chamber. In-situ RToF mass spectrometry is utilized to monitor the NCs sizes, and the average diameter for NCs is kept at 2 nm. The flux of NCs is measured by a quartz crystal microbalance (QCM), and the coverage is controlled by the deposition time under a constant NCs flux. In this study, the coverage of NCs was kept at 1.5 and 12 atomic monolayer (1 ML is equivalent to $1*10^{15}$ atoms per cm^2 deposited as NCs). Pure Pt and Ni NCs analogues of $Pt_{0.75}Ni_{0.25}$ NCs were also fabricated for control experiments using pure Pt and Ni plate targets and following the aforementioned synthesis method.

Structural and Morphological Characterization

Scanning transmission electron microscopy

$Pt_{0.75}Ni_{0.25}$ NCs deposited on TEM grids with 0.1 ML coverage were examined using a CS corrected JEOL ARM200F Microscope in STEM-HAADF mode operating at 200 keV. Elastically scattered electrons were collected using the HAADF detector with inner-outer collection angles of 68 mrad to 280 mrad. $Pt_{0.75}Ni_{0.25}$ NCs deposited on PANI electrodes at 1.5 and 12 ML coverages were directly investigated by SEM. Samples were imaged at the Leuven Nanocentre using the Raith GmbH EBL system equipped with a Zeiss GEMINI optical column. The accelerating voltage was set to 10 kV and an in-lens detector was used.

X-ray absorption fine structure spectroscopy

XAFS data of $Pt_{0.75}Ni_{0.25}$ and pure Ni NCs deposited on SiO_2/Si wafers with similar coverage were collected at the Dutch-Belgian Beamline DUBBLE (BM26A) of The European Synchrotron (ESRF), operating in uniform mode, with a current of 160–200 mA.[59] Data were collected at Ni K edge in fluorescence mode up to a wave number k = 10.5 $Å^{-1}$ with typical acquisition times of 25 min (i.e. 1-25 s per data point). Three spectra were averaged to improve the signal-to-noise ratio. Nickel foil and Nickel oxide were measured and used as references. Fitting of the EXAFS (extended X-ray absorption fine structure) experiment data was performed in the R range of 1-4 Å. Data reduction of the experimental X-ray absorption spectra was performed with the EXBROOK program.[60] Background subtraction and normalization were carried out by fitting (i) a linear polynomial to the pre-edge region in order to remove any instrumental background and (ii) cubic splines simulating the absorption coefficient from an isolated atom to the post-edge region. EXAFS refinements were performed with the EXCURVE package. [60] Phase shifts and backscattering factors were calculated ab initio using Hedin-Lundqvist potentials.

X-ray photoelectron spectroscopy

XPS data for $Pt_{0.75}Ni_{0.25}$, pure Pt and pure Ni NCs deposited on SiO_2/Si wafers were collected at room temperature and under UHV conditions (base pressure 1.6×10^{-9} mbar) in a Kratos Axis Supra system with a monochromatized Al Kα X-ray source (1486.6 eV) operated at 10 mA. High resolution XPS spectra were collected by a hemispherical analyser with passing energy of 20 eV. The spectra were aligned to the adventitious carbon peak C 1s placed at 284.8 eV. The deconvolution and fitting of the peaks were done with CasaXPS software.[61] The following spin-orbit coupling constraints were considered: peak separations of 17.3 eV and 3.35 eV and peak area ratios of 1/2 and 3/4 for Ni 2p and Pt 4f, respectively.

Electrochemical and electrocatalytic measurements

Electrochemical experiments such as EIS and CV were performed by VSP potentiostat/galvanostat (BioLogic Science Instruments). A standard three-electrode cell was used. The working electrode was a 0.78 cm^2 circular area on the PANI electrode directly deposited with Pt, Ni and $Pt_{0.75}Ni_{0.25}$ NCs. A homemade quasi Ag/AgCl electrode and a Pt wire were used as the reference and the counter electrode, respectively. All the potentials reported here are recorded versus Ag/AgCl reference electrode. All the electrochemical measurements were performed in 0.1M PBS, pH 7.2 at room temperature. The electrochemical surface area (ECSA) was calculated using the Randles-Servick equation.

Conflicts of interest

There are no conflicts to declare.

Acknowledgements

The authors gratefully acknowledge funding support from European Union's Seventh Framework Programme (FP7/2007-2013) under grant agreement no. 607417 (Catsense), KU Leuven Research Council (CELSA/18/032), Research Foundation - Flanders (FWO) (G.0B39.15), Flemish Hercules Stichting project (AKUL/13/19), EPSRC (EP/M028267/1), the European Regional Development Fund through the Welsh Government (80708), Israel Science Foundation (grant No. 1616/17). The experiments 26-01-1087 were performed on DUBBLE-BM26A beamline of The European Synchrotron (ESRF), Grenoble, France. Access to DUBBLE was arranged through the general support of the Research Foundation - Flanders (FWO) for the use of central facilities. The authors thank the staff of DUBBLE beamline of for their assistance and technical support and Prof. Jin Won Seo (KU Leuven) for assistance in STEM.

References

1. R. D. O'Neill, S.-C. Chang, J. P. Lowry and C. J. McNeil, *Biosens. Bioelectron.*, 2004, **19**, 1521-1528.
2. A. Kuzume, U. Zhumaev, J. Li, Y. Fu, M. Füeg, M. Estévez, Z. Borjas, T. Wandlowski and A. Esteve-Nuñez, *PCCP*, 2014, **16**, 22229-22236.
3. W.-C. Lee, K.-B. Kim, N. G. Gurudatt, K. K. Hussain, C. S. Choi, D.-S. Park and Y.-B. Shim, *Biosens. Bioelectron.*, 2019, **130**, 48-54.
4. L. Zhang, W. Du, A. Nautiyal, Z. Liu and X. Zhang, *Sci. China Mater.*, 2018, **61**, 303-352.
5. J. G. Ibanez, M. E. Rincón, S. Gutierrez-Granados, M. h. Chahma, O. A. Jaramillo-Quintero and B. A. Frontana-Uribe, *Chem. Rev.*, 2018, **118**, 4731-4816.
6. S. Bhadra, D. Khastgir, N. K. Singha and J. H. Lee, *Prog. Polym. Sci.*, 2009, **34**, 783-810.
7. M. H. Naveen, N. G. Gurudatt and Y.-B. Shim, *App. Mater. Today*, 2017, **9**, 419-433.
8. W. Yan, X. Feng, X. Chen, W. Hou and J. J. Zhu, *Biosens. Bioelectron.*, 2008, **23**, 925-931.
9. D. Li, J. Huang and R. B. Kaner, *Acc. Chem. Res.*, 2009, **42**, 135-145.
10. J. Shklovsky, A. Reuveny, Y. Sverdlov, S. Krylov and Y. Shacham-Diamand, *Microelectron. Eng.*, 2018, **199**, 58-62.
11. T.-H. Le, Y. Kim and H. Yoon, *Polymers*, 2017, **9**, 150.
12. C. Dhand, M. Das, M. Datta and B. D. Malhotra, *Biosens. Bioelectron.*, 2011, **26**, 2811-2821.
13. J.-M. Moon, N. Thapliyal, K. K. Hussain, R. N. Goyal and Y.-B. Shim, *Biosens. Bioelectron.*, 2018, **102**, 540-552.
14. K. Grennan, A. J. Killard, C. J. Hanson, A. A. Cafolla and M. R. Smyth, *Talanta*, 2006, **68**, 1591-1600.
15. H. Wang, J. Lin and Z. X. Shen, *Journal of Science: Advanced Materials and Devices*, 2016, **1**, 225-255.
16. J. Yuan, D. Han, Y. Zhang, Y. Shen, Z. Wang, Q. Zhang and L. Niu, *J. Electroanal. Chem.*, 2007, **599**, 127-135.
17. J. Wu and L. Yin, *ACS Appl. Mater. Interfaces*, 2011, **3**, 4354-4362.
18. W. Gao, S. Sattayasamitsathit, J. Orozco and J. Wang, *J. Am. Chem. Soc.*, 2011, **133**, 11862-11864.
19. X. Feng, C. Mao, G. Yang, W. Hou and J.-J. Zhu, *Langmuir*, 2006, **22**, 4384-4389.
20. A. Saheb, J. A. Smith, M. Josowicz, J. Janata, D. R. Baer and M. H. Engelhard, *J. Electroanal. Chem.*, 2008, **621**, 238-244.
21. C. O. Baker, B. Shedd, R. J. Tseng, A. A. Martinez-Morales, C. S. Ozkan, M. Ozkan, Y. Yang and R. B. Kaner, *ACS Nano*, 2011, **5**, 3469-3474.
22. A. Drury, S. Chaure, M. Kröll, V. Nicolosi, N. Chaure and W. J. Blau, *Chem. Mater.*, 2007, **19**, 4252-4258.
23. S. S. Barkade, J. B. Naik and S. H. Sonawane, *Colloids and Surfaces A: Physicochemical and Engineering Aspects*, 2011, **378**, 94-98.
24. Y. Bu and Z. Chen, *ACS Appl. Mater. Interfaces*, 2014, **6**, 17589-17598.
25. Q. Wang, X. Jing, J. Han, L. Yu and Q. Xu, *Mater. Lett.*, 2018, **215**, 65-67.
26. L. Yang, Y. Tang, D. Yan, T. Liu, C. Liu and S. Luo, *ACS Appl. Mater. Interfaces*, 2016, **8**, 169-176.
27. M. Pacini and D. W. Hatchett, *Electrochim. Acta*, 2018, **292**, 602-613.
28. M. Govindasamy, V. Mani, S. M. Chen, A. Sathiyan, J. P. Merlin and G. Boopathy, *Int. J. Electrochem. Sci.*, 2016, **11**, 10806-10814.
29. A. Houdayer, R. Schneider, D. Billaud, J. Ghanbaja and J. Lambert, *Synth. Met.*, 2005, **151**, 165-174.
30. J. Han, M. Wang, Y. Hu, C. Zhou and R. Guo, *Prog. Polym. Sci.*, 2017, **70**, 52-91.
31. S. Kumar, Sarita, M. Nehra, N. Dilbaghi, K. Tankeshwar and K.-H. Kim, *Prog. Polym. Sci.*, 2018, **80**, 1-38.
32. U. Bogdanović, I. Pašti, G. Ćirić-Marjanović, M. Mitrić, S. P. Ahrenkiel and V. Vodnik, *ACS Appl. Mater. Interfaces*, 2015, **7**, 28393-28403.
33. D. N. Nguyen and H. Yoon, *Polymers*, 2016, **8**, 118.
34. J. M. Kinyanjui, N. R. Wijeratne, J. Hanks and D. W. Hatchett, *Electrochim. Acta*, 2006, **51**, 2825-2835.
35. D. W. Hatchett, T. Quy, N. Goodwin and N. M. Millick, *Electrochim. Acta*, 2017, **251**, 699-709.
36. S. Jafarzadeh, E. Thormann, T. Rönnevall, A. Adhikari, P.-E. Sundell, J. Pan and P. M. Claesson, *ACS Appl. Mater. Interfaces*, 2011, **3**, 1681-1691.
37. V. Tsakova, *J. Solid State Electrochem.*, 2008, **12**, 1421-1434.
38. V. V. Kondratiev, V. V. Malev and S. N. Eliseeva, *Russ. Chem. Rev.*, 2016, **85**, 14-37.
39. A. Choudhury, *Sens. Actuators B Chem.*, 2009, **138**, 318-325.

40. L.-L. Guo, L.-J. Qin, B. Xu, X.-Z. Wang, C.-C. Hsueh and B.-Y. Chen, *Biochem. Eng. J.*, 2019, **148**, 57-64.
41. Y. Liu, K. Ai and L. Lu, *Chem. Rev.*, 2014, **114**, 5057-5115.
42. R. Ouyang, J. Lei, H. Ju and Y. Xue, *Adv. Funct. Mater.*, 2007, **17**, 3223-3230.
43. T. Łuczak, *Electrochim. Acta*, 2008, **53**, 5725-5731.
44. J.-l. Wang, B.-c. Li, Z.-j. Li, K.-f. Ren, L.-j. Jin, S.-m. Zhang, H. Chang, Y.-x. Sun and J. Ji, *Biomaterials*, 2014, **35**, 7679-7689.
45. A. N. Mansour and C. A. Melendres, *J. Phys. Chem. A*, 1998, **102**, 65-81.
46. A. N. Mansour, C. A. Melendres, M. Pankuch and R. A. Brizzolara, *J. Electrochem. Soc.*, 1994, **141**, L69-L71.
47. E. Choi, S. J. Oh and M. Choi, *Phys. Rev. B*, 1991, **43**, 6360-6368.
48. J. R. Aggas, W. Harrell, J. Lutkenhaus and A. Guiseppi-Elie, *Nanoscale*, 2018, **10**, 672-682.
49. W. W. Focke and G. E. Wnek, *J. Electroanal. Chem. Interf. Electrochem.*, 1988, **256**, 343-352.
50. S. Schindler and T. Bechtold, *J. Electroanal. Chem.*, 2019, **836**, 94-101.
51. X. Tuaev, S. Rudi, V. Petkov, A. Hoell and P. Strasser, *ACS Nano*, 2013, **7**, 5666-5674.
52. A. M. Gómez-Marín and J. M. Feliu, *Electrochim. Acta*, 2013, **104**, 367-377.
53. M. J. T. C. van der Niet, N. Garcia-Araez, J. Hernández, J. M. Feliu and M. T. M. Koper, *Catal. Today*, 2013, **202**, 105-113.
54. L. Jacobse, Y.-F. Huang, M. T. M. Koper and M. J. Rost, *Nat. Mater.*, 2018, **17**, 277-282.
55. A. M. Gómez-Marín and J. M. Feliu, *Electrochim. Acta*, 2012, **82**, 558-569.
56. P. P. Lopes, D. Strmcnik, D. Tripkovic, J. G. Connell, V. Stamenkovic and N. M. Markovic, *ACS Catal.*, 2016, **6**, 2536-2544.
57. T.-W. Liao, A. Yadav, K.-J. Hu, J. van der Tol, S. Cosentino, F. D'Acapito, R. E. Palmer, C. Lenardi, R. Ferrando, D. Grandjean and P. Lievens, *Nanoscale*, 2018, **10**, 6684-6694.
58. P. Ferrari, J. Vanbuel, Y. Li, T.-W. Liao, E. Janssens and P. Lievens, in *Gas-Phase Synthesis of Nanoparticles*, ed. W. V. V. G. Co, 2017, DOI: 10.1002/9783527698417.ch4, pp. 59-78.
59. M. Borsboom, W. Bras, I. Cerjak, D. Detollenaere, D. Glastra van Loon, P. Goedtkindt, M. Konijnenburg, P. Lassing, Y. K. Levine, B. Munneke, M. Oversluizen, R. van Tol and E. Vlieg, *J. Synchrotron Radiat.*, 1998, **5**, 518-520.
60. J. C. N. Binsted , S. J. Gurman and P. C. Stephenson 1991.
61. R. Hesse, P. Streubel and R. Szargan, *Surf. Interface Anal.*, 2005, **37**, 589-607.

Table of Content

Designed fabrication of flexible metal alloy nanocluster-polyaniline hybrid materials for efficient (bio)electrochemical applications.